university of groningen

University Medical Center Groningen

University of Groningen

An H I absorbing circumnuclear disk in Cygnus A

Struve, C.; Conway, J. E.

Published in:
Astronomy and astrophysics

DOI:
10.1051/0004-6361/200913572

IMPORTANT NOTE: You are advised to consult the publisher's version (publisher's PDF) if you wish to cite from it. Please check the document version below.

Document Version
Publisher's PDF, also known as Version of record

Publication date:
2010

Link to publication in University of Groningen/UMCG research database

Citation for published version (APA):
Struve, C., & Conway, J. E. (2010). An H I absorbing circumnuclear disk in Cygnus A. Astronomy and astrophysics, 513, A10. [A10]. https://doi.org/10.1051/0004-6361/200913572

Copyright
Other than for strictly personal use, it is not permitted to download or to forward/distribute the text or part of it without the consent of the author(s) and/or copyright holder(s), unless the work is under an open content license (like Creative Commons).

Take-down policy
If you believe that this document breaches copyright please contact us providing details, and we will remove access to the work immediately and investigate your claim.

Downloaded from the University of Groningen/UMCG research database (Pure): http://www.rug.nl/research/portal. For technical reasons the number of authors shown on this cover page is limited to 10 maximum.

Download date: 30-06-2019

Astronomy & Astrophysics manuscript no. struve
October 29, 2009
© ESO 2009

arXiv:0910.5705v1 [astro-ph.CO] 29 Oct 2009

An atomic circumnuclear disk in Cygnus A

C. Struve[1] and J.E. Conway[2]

[1] Netherlands Foundation for Research in Astronomy, Postbus 2, 7990 AA, Dwingeloo, The Netherlands
Kapteyn Institute, University of Groningen, Landleven 12, 9747 AD, Groningen, The Netherlands
e-mail: struve@astron.nl,
[2] Onsala Space Observatory, SE-439 92 Onsala, Sweden
e-mail: john.conway@chalmers.se

Received ???; accepted ???

ABSTRACT

We present Very Long Baseline Array (VLBA) H I absorption observations of the core region of the powerful radio galaxy Cygnus A. These data show both broad (FWHM = 244 ± 22km s^{-1}) and narrow (FWHM < 30km s^{-1}) velocity components. Modeling of the broad velocity absorption shows high opacity on the counter-jet, low opacity against the core and no absorption on the jet side; we argue this is most naturally explained by a circumnuclear H I disk orientated roughly perpendicular to the jet axis. We estimate that the H I absorbing gas lies at a radius of ∼ 80 pc and has a scale height of about 20 pc. We estimate this gas has a minimum density $n > 10^4$ cm^{-3} and a total column density in the range $10^{23} - 10^{24}$ cm^{-2}; we cannot however determine whether it is primarily an atomic or molecular phase. We find that this gas component does not cover the radio core in Cygnus A and therefore does not contribute to the total gas column that blocks our view of the hidden quasar nucleus. If however we were observing Cygnus A from a different direction it could add significantly. This implies that in some radio galaxies gas on ∼ 100 pc scales may contribute to the obscuration of the central engine. We argue that the circumnuclear torus in Cygnus A contains too little mass to power the AGN over > 10^7 yr but that material in the outer H I absorbing gas disk can provide a reservoir to fuel the AGN and replenish torus clouds. The second narrow H I absorption component is significantly redshifted (by 180km s^{-1}) with respect to the systemic velocity and probably traces infalling gas which will ultimately fuel the source. This component could arise either within a tidal tail structure associated with a recent (minor) merger or be associated with an observed infalling giant molecular cloud.

Key words. galaxies: active – galaxies: elliptical – galaxies: individual (Cygnus A) – galaxies: kinematics and dynamics – galaxies: structure – galaxies: ISM

1. Introduction

Circumnuclear obscuring tori/disks are an essential component of unified schemes of active galactic nuclei (e.g. Antonucci, 1993; Tadhunter, 2008). Recently there has been much progress in obtaining direct evidence for such structures especially in Seyfert luminosity objects. This includes modeling of the IR SEDs from AGN heated dust in clumpy tori (Nenkova et al., 2008b) and direct IR interferometric imaging of this dust on 1 pc - 10 pc scales (Jaffe et al., 2004; Tristram et al., 2009).

On larger scales adaptive optics IR observation of molecular hydrogen lines (Hicks et al., 2009) has revealed geometrically thick gas at radii 30 pc in Seyferts. Millimetre interferometery also detects molecular gas in emission on scales $r = 70$ pc (e.g. Schinnerer et al., 2000) albeit in more flattened disk like structures. Such outer disk structures may be continuous with inner obscuring tori and provide both the fuel and a conduit for feeding of the central engine. The relationship between these circumnuclear disks and obscuring tori is, however, far from clear.

Radio observations provide another means to study the circumnuclear gas environment. This can for instance be achieved by VLBI observations of maser emission from molecular gas (Lo, 2005), free-free absorption from ionised gas and absorption from atomic gas (H I). Examples of the use of the latter two tracers include observations of NGC 1275 (e.g. Vermeulen et al., 1994), Centaurus A (e.g. Jones et al., 1996; Morganti et al., 2008), Hydra A (e.g. Taylor, 1996), NGC 4261 (van Langevelde et al., 2000; Jones et al., 2001) and 1946 + 708 (Peck & Taylor, 2001). Because of their high spatial resolution such radio observations are especially suitable for studying circumnuclear obscuring matter in powerful narrow line radio galaxies which are expected (see Tadhunter, 2008) to be unified via orientation with radio-loud quasars. There is strong evidence from X-ray observations (Hardcastle et al., 2009) for the expected obscuration by large column densities in the former objects, however they are usually too distant and faint for optical and IR observations to directly observe the circumnuclear gas.

A prime target for studies of circumnuclear gas in a luminous 'hidden quasar' radio galaxy is the closest Fanaroff-Riley (Fanaroff & Riley, 1974) type II (FR-II) radio-galaxy Cygnus A. Spectropolarmetric observations of this source which revealed a hidden BLR in scattered light (Ogle et al., 1997) were a major milestone in the general acceptance of the orientation unfication scheme for powerful radio galaxies and radio-loud quasars. Further evidence for shadowing from a central torus comes from the bi-cones observed in both optical emission lines (Jackson et al., 1998) and IR continuum (Tadhunter et al., 1999). The sharpness of the edges of these bi-cones suggest that the inner face of any torus occurs at radii < 50 pc from the central engine (Tadhunter, 2008). Tadhunter et al. (2003) have measured the rotation curve from gas rotating around the bi-cone/radio-jet axis at $r \approx 300 - 1000$ pc using optical/IR emission lines allowing a central black hole mass to be estimated. These observations may trace the outer parts of a circumnuclear gas structure which connects with the inner obscuring torus. The ultimate origin of

this material could be related to the merger activity detected in Cygnus A (Canalizo et al., 2003).

The central radio core and inner jets of Cygnus A are relatively bright from millimetre to centimetre wavelengths allowing searches in absorption to constrain circumnuclear gas properties on small (< 100 pc) scales. Molecular absorption observations are ambiguous with so far only upper limits or marginal detections being reported (see e.g. Barvainis & Antonucci, 1994; Fuente et al., 2000; Salomé & Combes, 2003; Impellizzeri et al., 2006). VLBI observations by Krichbaum et al. (1998) however found evidence for ionised circumnuclear gas on scales < 20 pc via the detection of free-free absorption toward the counter-jet. Additionally Conway & Blanco (1995) detected broad H I absorption toward the core in VLA observations, which was interpreted in terms of a circumnuclear disk/torus model, with the H I absorption either tracing the small atomic fraction of a mainly molecular medium or a purely atomic structure. To better constrain the scale and geometry of this H I absorbing gas we have performed high resolution NRAO Very Long Baseline Array (VLBA[1]) H I absorption observations. A short report on a initial reduction of this data was given by Conway (1999), this present paper presents a fuller re-analysis of the data. The organisation of this paper is as follows, in Sect. 2 we describe the observations, while Sect. 3 presents the observational results including modeling of opacity profiles along the source. A discussion of the results is given in Sect. 4 and a summary in Sect. 5. At the redshift of Cygnus A ($z = 0.056$) for cosmologies with $H_o = 73$ km s^{-1} 1 mas corresponds to about 1 pc, which we adopt throughout this paper. All velocities quoted are heliocentric (optical definition).

2. Observations

Observations were performed on August 31st 1995 using the ten stations of the VLBA plus the phased VLA. Two IFs (left and right circular polarisation) with a bandwidth of 12.5 MHz and 256 channels were centered at the frequency of the previously observed H I absorption (∼ 1340 MHz, Conway & Blanco, 1995). A number of bright compact sources were observed as fringe finders and for bandpass calibration. The data were correlated in Soccoro, USA. A standard data reduction using AIPS was performed including fringe fitting, calibration and flagging of the data. Cygnus A lies at a relatively low galactic latitude ($b = 5.^\circ7$) and the effects of interstellar scattering are significant at VLBI resolution. For this reason four antennas which participated only in long baselines, namely Brewster, Hancock, Mauna Kea and St. Croix showed no fringes to Cygnus A and so were deleted from the subsequent data analysis. Initial amplitude calibration was accomplished for VLBA antennas using the recorded system temperature values (which took into account the dominant contribution to the noise from the lobes of Cygnus A). For the phased VLA the calibrator T_{ant}/T_{sys} values were used with a correction applied to take into account the system noise contribution from Cygnus A. Offsets in the VLA amplitude calibration scale were then corrected by comparing the correlated Cygnus A flux densities on long baselines to respectively the VLA and Pie Town. Initial continuum images were made via iterative phase self-calibration/deconvolution starting form an initial point source. A couple of cycles of amplitude and phase self-calibration were performed at the very end to obtain a noise limited continuum map.

Extensive experiments were carried out to determine the optimum uv weighting which gave the best combination of sensitivity and resolution for both continuum and spectral line. Final images were made using uniform weighting with robustness factor 0.5; giving rise to an almost circular dirty beam with main lobe width FWHM ≈ 25 mas. Since the uv point weights also took into account the sensitivity of each baseline (by weighting by 1/noise variance) the final continuum and spectral line images are dominated by the baselines to the VLA. CLEAN images were restored with a circular FWHM 25 mas Gaussian; however the effective image resolution is less than this because of the effects of foreground interstellar scattering. The observed effective resolution (i.e. the clean beam convolved with the interstellar scattering) is 32.7 mas, as determined by measuring the FWHM of the continuum profile perpendicular to the jet at the core position - implying an interstellar scattering contribution of 21 mas.

The resulting continuum image (see Fig. 1) has rms noise of 0.43 mJy beam^{-1} and shows besides the unresolved core a jet and counter-jet structure (see Sect. 3). In principal, the counter-jet structure can be an artifact of phase self-calibration starting from a point source. To check this possibility we re-mapped the data only allowing flux density on the jet side to be included in the model in the initial cycles, but in all cases emission on the counter-jet side remained. The existence of a counter-jet is also confirmed by other observations (e.g. Krichbaum et al., 1998). In making our final continuum and spectral line images we used data self-calibrated against continuum models including both jet and counter-jet emission. Before making our spectral line cube we removed the continuum contribution using the AIPS task UVLIN and then imaged using the same weighting as used for our continuum image and used the same CLEAN restoring beam. In order to increase sensitivity when creating our spectral line cube the uv data were averaged in frequency to give a final channel separation equivalent to 14.8 km s^{-1} in velocity or a velocity resolution of 29.6 km s^{-1} after Hanning smoothing. The noise achieved in the final line cube was $\sigma_{rms} = 2.36$ mJy beam^{-1} per channel.

3. Results

3.1. Continuum image

The 1340 MHz continuum image (Fig. 1, top panel) is very similar to the 1660 MHz image shown by Krichbaum et al. (1998). We clearly detect the unresolved core, the jet and the weaker counter-jet (SE of the core). The PA of the jet is $105^\circ \pm 2^\circ$, in agreement with VLBI observations at higher frequencies (Krichbaum et al., 1998) and the kpc-size jet structure (Carilli et al., 1991). The continuum peak is 0.16 Jy beam^{-1}, the total continuum flux recovered in our observations is 0.50 Jy.

3.2. H I absorption

An integrated absorption spectrum over our spectral line cube is shown in Fig 1, bottom left. Broad (FWHM Δv = 456 km s^{-1}) H I absorption is detected in the range from 16679 to 17135 km s^{-1}, with the peak being located at $v = 17002$ km s^{-1}. The integrated spectrum is well fitted by two Gaussian components, yielding centroid velocities of 16923 ± 11 and 16996 ± 5 km s^{-1}, with FWHM= 244±22 and 31±11 km s^{-1} respectively.

[1] The VLBA is operated by the National Radio Astronomy Observatory which is a facility of the National Science Foundation operated under cooperative agreement by Associated Universities, Inc.

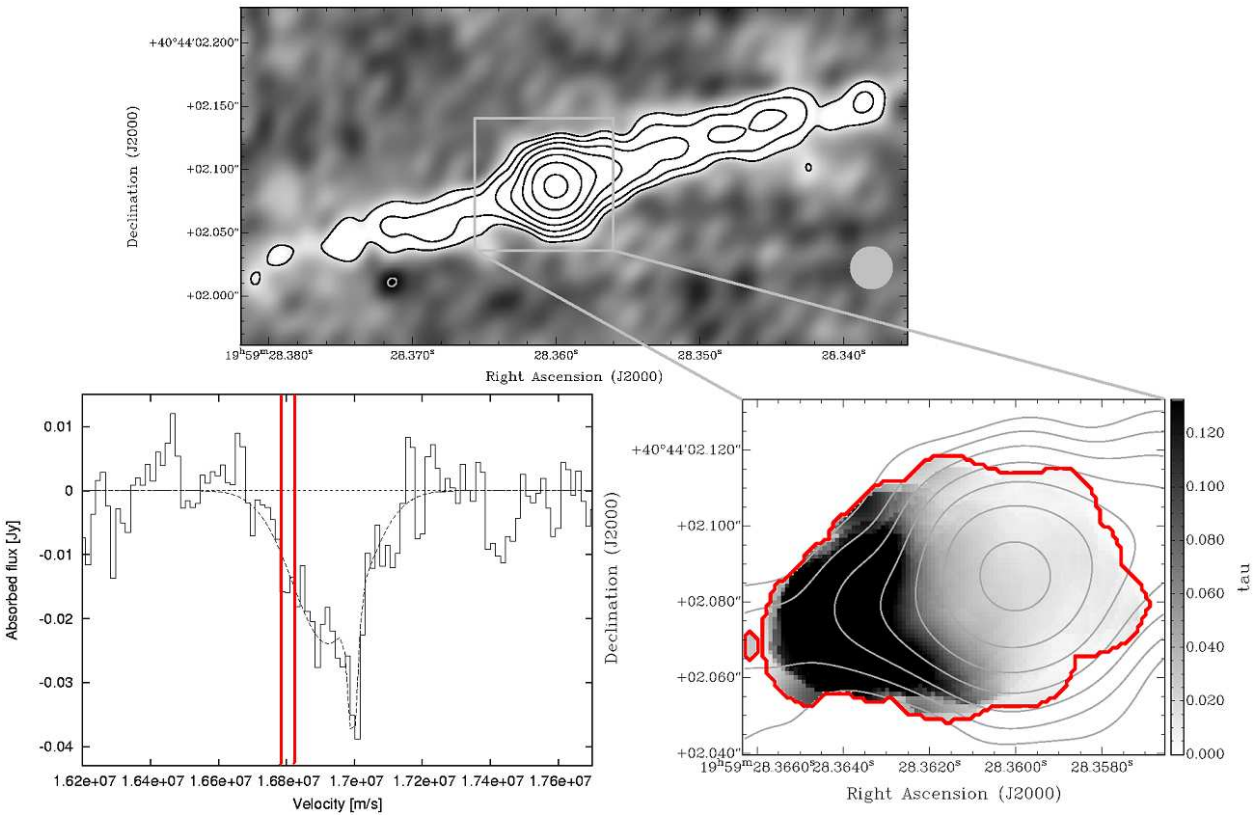

Fig. 1: Top panel: Continuum image at 1340 MHz. The lowest contour is at 2 mJy beam^{-1} with subsequent contours increasing by a factors of 2. The effective beam FWHM (combination of restoring beam and interstellar scattering, see Sect. 2) is indicated in the lower right corner. Bottom left panel: Integrated absorption spectrum from blanked cube. The dashed line shows the two component Gaussian fit. The vertical lines indicate the redshift range for the grayscale opacity image shown in the bottom right panel. Bottom right panel: Contours show continuum. Grayscale shows the mean opacity over the velocity range indicated in the bottom left panel. The thick dark line shows the un-blanked region over which the integrated absorption spectra (shown in the bottom left panel) is calculated.

The second, narrow component has a FWHM velocity width similar to our velocity resolution and hence we consider this velocity width as an upper limit of the true line width. The presence of two components in the integrated spectrum suggests that the H I absorption consists of two different, overlapping structures. Despite small differences in the flux scale (continuum and absorption spectrum), the VLBA data agree in absorption width and profile shape with the VLA A- and B-array observations of Conway & Blanco (1995). This close similarity suggests that we have recovered the full absorption seen by the VLA. The difference seen in flux scale between our VLBI and the published VLA observations are likely due to inaccuracies in amplitude calibrations of the VLA. This instrument, unlike VLBI, does not record the antenna system temperatures which are greatly enhanced due to the presence of the bright radio lobes of Cygnus A in the primary beam of each antenna, complicating the amplitude calibration.

Inspection of the data cube shows that the absorption is spatially resolved and is detectable over 95 mas in angle along the radio axis (i.e. $\sim$ 3 effective beam FWHM's). Below the second contour of the continuum image it is not possible to constrain the H I absorption because the background is too weak. The deepest absorption measured in mJy is toward the counter-jet and unresolved core but the highest opacities occur for the broad velocity component on the counter-jet side (see Fig. 1, bottom right). We find no indication of changes in spectral line absorption profiles in directions perpendicular to the jet axis - this is as expected given the small jet width (Krichbaum et al., 1998). Compared to our effective resolution, this means we need to only consider the spectral profile as a function of position along the jet axis as shown in Fig. 2. In this figure the top panel shows the rotated continuum image while the middle panel shows the absorbed flux density (contours) and absorbed flux/continuum ratio (colours) versus velocity and position along the jet.

The highest contours belong to the narrow velocity absorption component at 16996 km s^{-1} seen against the core, a slight extension on the jet-side is detectable, consistent with having the same $\tau \approx 0.1$ opacity as seen on the core. Because of the rapid fall-off of continuum intensity along the jet and counter-jet further information about the spatial distribution of the narrow velocity component is limited.

The broad absorption component in Fig. 2, middle panel (seen between velocities 16996 km s^{-1}and 17000 km s^{-1}), is detected from the core position out to 65 mas along the counter-jet. Over this spatial range the broad component has absorbed flux densities (contour levels) which stay almost constant; given the rapid fall off in background continuum this corresponds to a rapid increase in line to continuum ratio (colours). Over the range of position from -50 mas to -65 mas spectra taken show the absorption to be flat bottomed and the absorbed flux density comparable with the continuum, both implying H I opacities $\tau \gg 1$. The absorption shows an apparent sharp decrease be-

yond −65 mas, though in a region with with very weak continuum (we discuss further the reality of this decrease in Sect 3.3). The broad absorption also apparently has a small but significant opacity ($\tau \approx 0.03$) at the position of the core, however, this may be due only to the limited spatial resolution causing "leakage" of absorption onto the core position. Quantitative estimates of broad line opacity along the source are made in Sect 3.3 where the above two points are addressed.

Reinforcing the above description of the two velocity components the bottom panel of Fig. 2 shows the line to continuum ratio averaged over different velocity ranges versus position. The solid line shows average line-to-continuum for velocity ranges where the broad component dominates, while the dashed line is for a velocity range where the narrow absorption is most dominant. The broad component shows rapidly increasing absorption along the counter-jet reaching a peak velocity averaged line-to-continuum ratio of almost 0.6 at −55 mas (with peak ratios within the velocity profile at this position in fact reaching up to 1 and beyond). The second profile (dashed line) for the velocity range where the narrow velocity component normally dominates has approximately the same mean opacity on the core and jet. On the counter-jet side the average opacity over this velocity range increases, this is however consistent with the narrow absorption component having the same opacity as on the core and jet-side but with the average line-to-continuum ratio becoming dominated by contamination from the high velocity wings of the broad velocity component.

3.3. Modelling spatial variations in broad line opacity

The increase in line-to-continuum ratio of the broad absorption seen on the counter-jet side (see Sect. 3.2 and Fig. 2) implies a rapid increase in opacity. As noted in Sect. 3.2, at the position of maximum absorption the spectral profiles are flat-bottomed and saturated implying large τ. To more accurately convert the line-to-continuum ratios versus velocity to peak opacity, and therefore estimate H I column density variations, we have carried out a detailed modeling of the data. In this modeling we estimate both continuum and peak opacity estimates on pixels separated by 15 mas (i.e. just under half an effectives beam FWHM width). Additionally by taking into account the effective beam width this modeling provides a modest super-resolution of the data, important because interstellar scattering limits our spatial resolution (Sect. 2). Specifically, we are interested in the question of whether the weak broad absorption apparently seen at the core position (see Fig. 1 bottom right panel) is real or whether it can be explained by the combination of very strong absorption on the counter-jet side combined with limited spatial resolution.

In our modeling we first made estimates for the underlying continuum profile at each pixel where there was detectable absorption. Continuum intensities were varied at each of the seven pixels until that after convolution with the effective restoring beam the model continuum profile versus position fitted the observations. In a similar way we next estimated for each pixel the absorbed line area (mJy km s^{-1}) at velocities in the range 16716 - 16980 km s^{-1} (where the broad absorption component dominates). Pixel values were again adjusted such that after convolution by the effective beam the model fitted the observations. Finally an estimate was made at each pixel of the peak of the spectrum of opacity versus velocity by combining the pixel-based continuum and spectral line absorption estimates. In doing this we assumed the broad-component opacity spectrum was Gaussian with fixed velocity centroid and fixed FWHM.

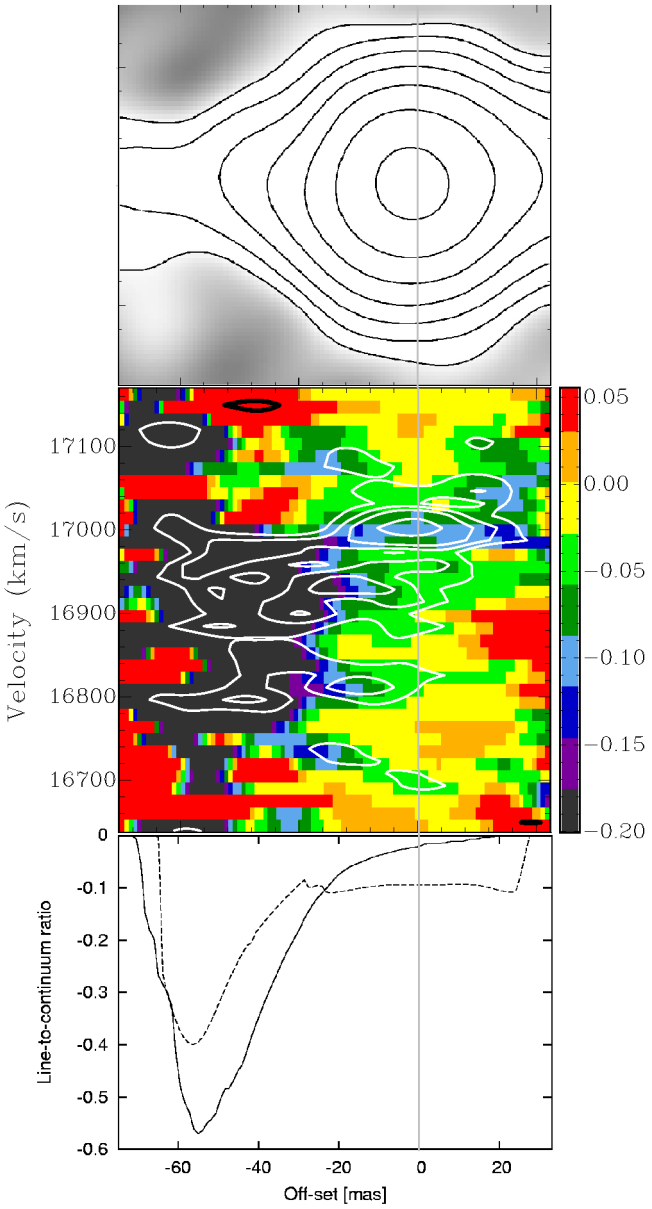

Fig. 2: Top panel: Radio continuum image of the core region rotated such that the jet is pointing to the right and the counter-jet to the left. Contour levels are the same as in Fig. 1. Middle panel: Position-velocity diagram along the radio axis. Colour scale shows the line-to-continuum ratio (note: saturated over 0.2). Over-plotted in contours is the absorbed flux density in mJy beam^{-1}. Contour levels are -15, -10, -7.5, -5.0 (white) and 5.0 mJy beam^{-1} (black). Bottom panel: Velocity averaged line-to-continuum ratio along the source for two different velocity ranges. The solid line is for a velocity range dominated by the broad velocity component (16716 – 16980 km s^{-1}), the dashed line for a velocity range (16981 – 17024 km s^{-1}) centred on the narrow absorption system velocity.

The resulting fits reproduce (see Fig. 3), to first order, both the observed continuum and the absorbed flux profiles along the source. Deviations of the fits from the data are likely due to the background continuum being more complicated (see Krichbaum et al., 1998) than our parameterisation of it. Table 1 gives our results and the line centre peak opacity is plotted in Fig. 4. We estimate the error of the line-to-continuum ratio

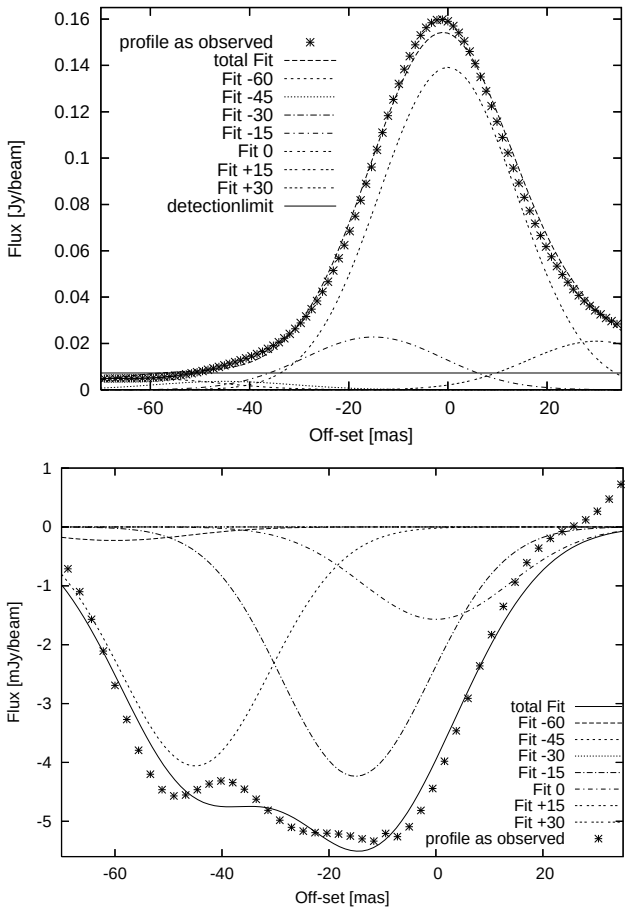

Fig. 3: Top panel: Comparison of model fit and data for the observed continuum profile found by adjusting pixel values while assuming an effective beam Gaussian beam of FWHM of 32.7 mas. Bottom panel: Comparison of model and data for average absorbed line flux over the broad component velocity range from 16716 – 16980 km s^{-1}(multiply by 264 km s^{-1}to get observed and modeled absorbed line profile area between these two velocity limits). In both plots negative offsets correspond to counter-jet, positive offsets to jet side. The corresponding pixel parameters for both fits are summarized in Tab. 1.

r (1)	F_C (2)	F_L (3)	$F_L F_C^{-1}$ (4)	τ_0 (5)
-60	4.73	0.23	0.05 ± 0.12	0.080 ± 0.210
-45	3.62	4.06	1.12 ± 0.15	> 3.300
-30	0.02	0.00	0.00	-
-15	22.78	4.24	0.19 ± 0.02	0.320 ± 0.040
0	139.16	1.57	0.01 ± 0.004	0.016 ± 0.006
15	0.00	0.00	-	-
30	20.98	0.00	0.00 ± 0.03	0 ± 0.0478

Table 1: Summary of results of modeling of continuum and broad absorption, see text for details. (1) Distance from the core (mas) of fitted pixel, negative offsets correspond to counter-jet, positive to jet side. (2) Fitted continuum brightness [mJy]. (3) Fitted mean absorbed flux [mJy] over frequency range. (4) Fitted line-to-continuum ratio. (5) Modeled peak opacity of spectral absorption. At $r = -45$ mas the given value is actually a lower limit as we subtracted 2σ from the line-to-continuum ratio.

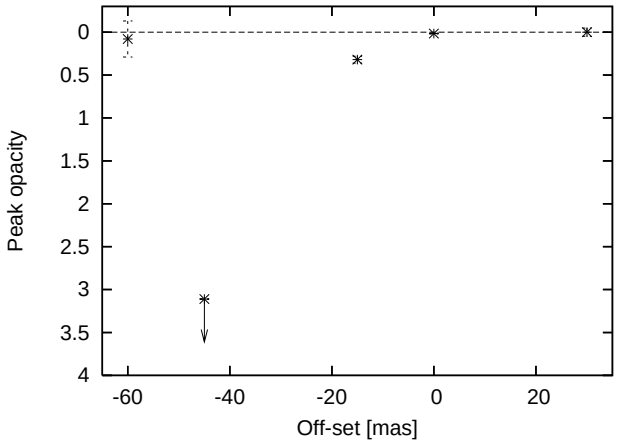

Fig. 4: Estimates of broad absorption component line opacity versus position along the radio axis after modeling. The opacities and errors plotted are taken from Tab. 1. No opacity is plotted at position -30 and +15 mas because the fitted continuum intensity at these positions was zero.

(Tab. 1, column 4) to soley depend on the rms in the line data. The peak opacity (column 5) takes into account that part of the absorption spectrum is flat bottomed and the attached error is calculated based on a $1\sigma_{\rm rms}$ uncertainty in our line data. Our results are consistent with no broad H I absorption on the jet-side and any opacity against the core being low (0.016). Moving outward from the core along the counter-jet, the opacity increases and peaks at 45 mas ($N_{\rm H\,I} = 1.6 \cdot 10^{21} T_{\rm spin}$) before it sharply decreases to 0.078 at 60 mas from the core. Based on uncertainty estimates of the absorbed flux, this drop in opacity is real and not an observational artifact (i.e. not due to insufficient signal-to-noise).

4. Discussion

4.1. A disk geometry for the broad absorption component

The fact that the broad velocity width absorption is seen at high opacity only against the counter-jet and not against the jet is similar to the situation found for other powerful cores of radio galaxies observed in H I absorption. Other examples include the FR-I sources Hydra A (e.g. Taylor, 1996) and NGC 4261 (van Langevelde et al., 2000). The most natural explanation for these observations is that the H I absorption lies in a flattened structure roughly in a plane perpendicular to the radio axis (i.e. a circumnuclear disk). Alternative explanations involving foreground clouds in the ISM of the host galaxy seem unlikely requiring within elliptical hosts a large covering factor of 10pc-100pc sized clouds with uncharacteristically large internal velocity dispersion (of order 300 km s^{-1}).

Converting our observations of the location and distribution of H I absorption along the counter-jet to an exact of radius in the disk depends on the precise orientation of the disk. However, over the range of plausible disk orientations this radius varies over a fairly narrow range, as can be seen by examining two limits, when the disk is close to edge-on and when at its maximum plausible tilt. In the first case the H I profile width in Fig. 4. measures the scaleheight of the disk. Since we know the central black hole mass ($M_{\rm BH} = 2.5 \cdot 10^9$ $M_\odot$, Tadhunter et al., 2003).

we can use the thin disk approximation to obtain the radius at which the H I absorption occurs. We use

$$\frac{\Delta h}{r} \sim \frac{\Delta v}{v_{\rm rot}(r)} \quad (1)$$

where Δh is the scaleheight, r the radius from the core, Δv = 104 km s^{-1} the velocity disperison (estimated from the Gaussian fit in Sect. 3.3) and $v_{\rm rot}(r)$ the rotation velocity at radius r, which is constrained by assuming Keplerian rotation around the central black hole. Assuming Δh = 25 pc and solving for r we obtain r = 85 pc. In the other limit we consider a maximally inclined disk. Based on VLBI observations of the jet to counter-jet brightness ratio of the parsec scale jet (Krichbaum et al., 1998), the jet axis is orientated at an angle $\theta > 80^\circ$ to the line of sight. Based on measured misalignments of larger scales (Tadhunter et al., 2003) we estimate a maximum misalignment between disk and radio axes of 30°- which gives a maximally inclined disk which is 40° from edge-on. The peak H I opacity is observed to occur at projected distance 45 pc along the counter-jet, when deprojected this corresponds to radius 70 pc. Using again eq. 1 this gives a scale height of $\sim$ 19 pc. Based on the above two limits we assume in the following that the H I peaks at a radius 80 pc from the black hole and has scaleheight of about 20 pc. The resulting opening angle of the circumnuclear H I disk is $\sim 14^\circ$ which is similar to what is found in other sources (e.g. in NGC 4261 van Langevelde et al., 2000).

An important question in considering the feasibility of the disk hypothesis is the velocity of the broad absorption relative to the systemic velocity of the galactic nucleus. For a disk which is perfectly normal to the jet axis theses velocities are expected to be the same. Estimating systemic velocities from optical/IR emission lines is however difficult because of the effects of obscuration and non-circular motions (in particular possible outflows in emission lines). According to Tadhunter et al. (2003) the most reliable estimate of the systemic velocity comes from space-based HST/STIS [O III] emission lines observations which give a range of 60 km s^{-1}from 16788 $\leq v_{\rm sys} \leq$ 16848 km s^{-1}. The centroid of the broad component at 16923 km s^{-1} is 105 km s^{-1} beyond the mean systemic velocity. The observed offset can however can be accommodated if there were a fairly modest misalignment between the disk axis and the jet. VLBI observations constrain the jet axis to be within 10° of the sky plane. For such an orientation misalignments between projected jet axis and disk axis will be similar to intrinsic misalignments. Given the arguments above that the H I absorption occurs at $\sim$ 80 pc radius and given the estimated central black hole mass of ($M_{\rm BH} = 2.5 \cdot 10^9$ M$_\odot$, Tadhunter et al., 2003), the orbital velocity is $v_{\rm rot}(r = 80{\rm pc})$ = 367 km s^{-1}. Given this orbital velocity a misalignment of only 19° is sufficient to explain the difference between the H I centroid and systemic velocities.

4.2. Physical properties of the broad absorption component gas

According to Maloney et al. (1996) the physical state of gas around an AGN is controlled by an ionisation parameter determined from the ratio of the hard X-ray photon flux to local gas density. At a given radius, r this ionisation parameter equals

$$\xi_{\rm eff} = L_{\rm X} \cdot n^{-1} \cdot r^{-2} \cdot N_{22}^{-0.9} \quad (2)$$

where $L_{\rm X}$ is the luminosity in > 2 keV X-rays and n is the gas number density. The final term takes account of the effects of X-ray photoelectric absorption where N_{22} is the the column density in units of 10^{22} cm^{-2} ($20.0N_{22}$ along the line of sight to the core from X-ray observations, Young et al., 2002). According to the model of Maloney et al. (1996, see Fig. 3) for Cygnus A at r = 80 pc the gas fraction is predominantly atomic (> 90%) for a density range $10^3 < n < 1.6 \cdot 10^5$ cm^{-3}. The remaining < 10% of the gas is ionised at low densities ($n = 10^3$ cm^{-3}) and becomes molecular at higher densities ($n \approx 10^5$ cm^{-3}). Above densities of $3.3 \cdot 10^5$ cm^{-3}) the gas is mostly molecular. The model can also be used to predict the H I and free-free absorption opacity to compare to observations and so constrain the density. These calculations of model opacities depend on the assumed path length through the absorbing gas. Based on our estimate of the disk thickness of 20 pc and the maximum disk inclination angle with respect to the line of sight (Sect. 4.1) we estimate this quantity to be at least 31 pc. This is a strict lower limit and we adopt $L_{\rm geom}$ = 40 pc as a more likely value. Note that if the gas exists in clouds the effective path length through absorbing gas can be less than $L_{\rm geom}$ but it cannot be larger.

Using the above assumptions we find that upper limits on free-free absorption do not give any useful gas density constraints. This is because although the free-electron fraction increases at low densities this is componsated for by a lower total gas column such that the 21cm free-free opacity against the counter-jet is less than 0.1 over all reasonable densities. For modeling H I absorption the relevant parameters given by Maloney et al. (1996) are the predicted gas temperature and atomic fraction versus effective ionisation parameter $\xi_{\rm eff}$. At the radius of the absorbing H I assuming densities high enough to give a predominately atomic column the increase of $T_{\rm spin}$ due to radiative excitation from the radio core is negligible (see e.g. Bahcall & Ekers, 1969) so we assume the atomic gas is thermalised so that its spin temperature ($T_{\rm spin}$) equals the gas temperature as given by Maloney et al. (1996). Assuming a uniform density along the geometric path $L_{\rm geom}$ the $\xi_{\rm eff}$ as a function of gas density n is given by eq. 1; where we take into account both the direct $1/n$ term and the increase in the shielding total column density toward the central X-ray sources ($N_{22} \approx nL_{\rm geom} \cdot 10^{-22}$ cm^{-2}). Combining all these quantities we can model $N_{\rm H\,I} \cdot T_{\rm spin}^{-1}$ versus gas density and compare to the observed value of $N_{\rm H\,I} \cdot T_{\rm spin}^{-1} = 1.6 \cdot 10^{21}$ cm^{-2}K^{-1}. We find that at densities $n < 10^4$ cm^{-3} (giving gas and spin temperatures > 740 K) we predict insufficient H I absorption to explain the observations, even if as we assume the whole 40 pc column is filled with atomic gas at this density. This sets a minimum density for the H I absorbing gas. At this minimum density the resulting total gas column along the line of sight is $N = 1.1 \cdot 10^{24}$ cm^{-2}.

For the gas density range $1.0 \cdot 10^4$ cm^{-3} $< n < 3.2 \cdot 10^4$ cm^{-3} there exist pure atomic phase gas solutions which fit the H I observations if the gas is in clouds whose line of sight filling factor $f_{\rm LOS}$ is much less that unity. In this regime the requirements on total gas column density are reduced, because at higher densities the gas/spin temperatures decline making hydrogen atoms more efficient at absorption. At the density boundary between having predominately atomic or molecular phase clouds (at density $4.6 \cdot 10^4$ cm^{-3}) the spin temperature is $\sim$ 114 K the cloud line of sight filling factor is $f_{\rm LOS} = 0.032$ and $N = 1.82 \cdot 10^{23}$ cm^{-2} which is comparable to the X-ray absorption column along the line of sight to the central engine. At higher densities the clouds become predominately molecular but our H I absorption results can still be fit assuming similar total column densities. The reason is that although the atomic fraction declines rapidly with increasing density the temperature also declines, increasing the ef-

ficiency of absorption for hydrogen atoms, almost exactly compensating.

In summary we cannot on the basis of our H I observations alone distinguish between models for the H I absorbing gas phase which are primarily atomic or molecular. We can however set at minimum density ($n > 10^4$ cm^{-3}) and a range for the total gas column density through the H I absorbing disk (10^{23} cm$^{-2} < N < 10^{24}$ cm^{-2}). Estimating total gas masses is complicated for those solutions invoking clouds in that these solutions only fix the line of sight filling factor, converting to volume filling factors requires knowing the cloud size, on which we have no constraints. In contrast for the minimum density solution where the gas column is continuous we can make a rough estimate of disk gas mass of $M_{\rm gasdisk} = 1.0 \cdot 10^8$ M$_\odot$ within the inner 80 pc radius of the disk. For higher density solutions, both total required column densities and cloud filling factors decrease so that total gas mass requirements are significantly less. In all cases the total disk mass is much less than that of the central black hole ($M_{\rm BH} = 2.5 \cdot 10^9$ M$_\odot$, Tadhunter et al., 2003) which therefore dominates the kinematics in the inner part of the nucleus that we observe.

4.3. Constraints on circumnuclear torus properties and relation to the H I disk

It is interesting that the estimated total gas column density through the H I absorbing gas (see Section 4.2) is comparable to that estimated by X-ray photoelectric absorption ($2 \cdot 10^{23}$ cm^{-2}, Young et al., 2002). Is it possible that most of this column density and most of the material that hides the quasar nucleus occurs as far out as $r = 80$ pc? An obvious problem with such a scenario is the absence of broad H I absorption along the direct line of sight to the radio core (peak opacity is $\tau_0 = 0.016 \pm 0,006$, compared to > 1 on the counter-jet, see Sect. 3.3 and Fig. 2). A change in gas physical state with scale-height in the disk while keeping almost constant column density can be considered as an explanation; however it seems that it can be dismissed. If the high scale-height gas covering the core were still predominately atomic or molecular we find no density solutions that fit the low limit on H I absorption seen. On the other hand if the high scale height gas were wholly ionised at this column density it would strongly free-free absorb the radio core. Although there are signs of free-free absorption at $r \leq 20$ pc (Krichbaum et al., 1998) along the counter-jet this absorption does not cover the core position itself.

It seems likely instead that most of the X-rays absorbing column in Cygnus A and other hidden quasars occurs on scales $\ll$ 100 pc in a compact circumnuclear *torus.* The inner radius of such a torus is set by the dust sublimation radius, $r_{\rm d} = 0.4 \cdot L_{\rm bol} \cdot 10^{-45}$ erg s^{-1} pc (Nenkova et al., 2008b) where $L_{\rm bol}$ is the AGN bolometric luminosity. For Cygnus A $L_{\rm bol}$ is estimated to be $1.5 \cdot 10^{45}$ erg s^{-1} (Whysong & Antonucci, 2004) giving $r_{\rm d} = 0.6$ pc. The outer radius ($r_{\rm out}$) is probably not as cleanly defined as in some early depictions of doughnut-like tori (Padovani & Urry, 1992) and may even be continuous with larger circumnuclear disks (see references in Sect. 1). Consistent with these more general geometries the term 'torus' can be thought of, if one prefers, as an acronym for 'Thick/toroidal Obscuration Required by Unified Schemes' (Conway, 1999; Elitzur, 2008) rather than referring to a specific fixed geometry.

Recently Privon (2009) has fitted the observed Spectral Energy Distribution (SED) of the Cygnus A nucleus with a combined synchrotron jet, starburst and torus model. The torus fitting assumed the clumpy model of Nenkova et al. (2008a,b). A wide range of solutions were obtained depending on assumptions about the disk inclination and synchrotron jet spectrum. Most plausible solutions however had cloud number density per unit volume declining as r^{-q} with $q = 1$ and ratios of outer to inner radius, $Y = 30$ (giving $r_{\rm out} = 18$ pc for Cygnus A). Satisfyingly the predicted total column density matches the X-ray absorption estimate within the errors. Despite the relatively large formal outer radius the concentration of clumps toward the inner edge means that most of the column density is concentrated at small radii. For a radial exponent of $q = 1$ half of the total column density occurs within $\sqrt{Y} \cdot r_{\rm in}$ corresponding to 3.2 pc, i.e. on a much smaller scale than our observed H I absorption.

The above results begs the question of relationship between the H I absorbing disk and the circumnuclear torus in Cygnus A. The mass in the torus is very low ($6 \cdot 10^5$ M$_\odot$, following Elitzur, 2008) and the lifetime of large scale height clouds within it is short (due to intercloud collisions, see e.g. Krolik & Lepp, 1989). Hence, both to fuel the quasar-like nucleus at the expected rate of $\sim$ 1 M$_\odot$yr^{-1} and to replenish the torus clouds a much larger reservoir of material is required, which could reside in the H I absorbing disk. The mass in such a disk (see Section 4.2) is sufficient to power the source for 10^7 to 10^8 yr and may form part of a 'feeding structure' which funnels gas from kilo-parsec scales into the central black hole. A feeding connection between disk and torus seems likely but the mechanisms of gas transport between the two scales is unclear.

Pertinent to the feeding question is whether the torus and the H I absorbing disk are a continuous structure with one gradually melding into the other, or if they are dynamically distinct and contain gas with very different physical conditions. The former possibility is motivated by the fitted torus outer radius $r_{\rm out} = 18$ pc which is of the same order of magnitude as the radius of the H I absorption ($r = 80$ pc). Furthermore the torus outer radius determined from SED fitting is not well constrained by the data and may extend beyond this limit. In such a continuous model with clouds with approximately fixed internal density extending out with low volume filling factor to 80 pc radius the gas would likely be in an increasingly molecular state over a projected radius from 1 to 70pc. It is hard to see how the rapid gradient in H I absorption seen along the counter-jet could be reproduced in such a case. Furthermore the observation of free-free absorption at intermediate positions ($r < 20$ pc, Krichbaum et al., 1998) is inconsistent with such a continuous model. It seems more likely that the torus — although ultimately fed from gas in the disk — is a distinct structure, perhaps generated in an accretion disk wind as in the model of Elitzur & Shlosman (2006). Clearly, more work is required to understand how the observed components in Cygnus A and other radio galaxies of 100 pc scale H I absorbing disks, inner ionised gas and circumnuclear tori are connected in self-consistent structures which both obscure and feed the central engine.

An additional remark concerning the disk/torus interrelationship is that although in Cygnus A the H I absorbing disk likely does not contribute to total absorbing column toward the central engine (as estimated from the X-ray observations) it could have done so if we had observed Cygnus A from a different direction. Hence it is possible that in a small fraction of radio galaxies part of the obscuration hiding the central engine occurs at 100pc scales as well as in a compact circumnuclear torus. In such objects the high ionisation narrow lines would be at least partly obscured possibly mimicking a low-ionization radio galaxy without a quasar nucleus.

Further progress on understanding the circumnuclear gas environment in Cygnus A probably requires the reliable detection of molecular absorption and its imaging with VLBI. Single dish searches at commonly observed molecular transitions such as the ground and higher rotational transitions of CO (Barvainis & Antonucci, 1994; Salomé & Combes, 2003) have so far yielded only upper limits. In contrast a tentative detection of CO+ in absorption using the IRAM 30m was reported by Fuente et al. (2000) with a centroid velocity and FWHM velocity width (170 km s^{-1}) very similar to that of our broad H I absorption. This detection has yet to be confirmed interferometrically (A. Fuente, private communication). Given the results in this paper, despite the similarity in spectral shape, it is highly unlikely that these observations are probing the same gas column as seen in H I absorption. The counter-jet which provides the background continuum against which the atomic hydrogen absorption is seen will have negligible flux density at millimetre wavelengths. Instead the line of sight probed at 3mm wavelength will probably lie at projected distances $<$ 1 pc from the central engine. While this is comparable to the scales on which the circumnuclear torus has its largest column density ($\sim$ 3 pc) we would expect that the velocity dispersion of clouds in such a geometrically thick torus would be comparable to the orbital velocity at this radius (i.e. 19000 km s^{-1}), which is much broader than is observed. Similar considerations apply to the tentative VLBA observations of exited OH absorption reported by Impellizzeri et al. (2006) at projected radii $<$ 3 pc which only have observed width $\sim$100 km s^{-1}.

4.4. The narrow absorption component

While we argue that the broad absorption component is caused by gas rotating around the black hole (Sect. 4.1), the narrow ($<$ 30 km s^{-1} see Sect. 3) absorption gas is likely to have a different origin. This narrow velocity component is significantly redshifted ($\sim$ 180 km s^{-1}) with respect to the optical systemic velocity implying foreground gas moving inward toward the nucleus. This component is detected over the whole continuum region where the observations are sensitive enough to detect an opacity of $\sim$ 0.1 (see Fig. 2). A very similar opacity and centroid velocity is seen at the core position and one effective beam away on the jet side. The apparent increase in opacity at the velocity of the narrow absorption that is seen on the counter-jet side in Fig. 2 can be explained entirely by contamination by the broad velocity wings of the broad velocity absorption. While we do not have many independent samples of the narrow velocity component opacity versus position those we do have are consistent with a constant narrow component opacity of 0.1 over the whole VLBI radio source. Although the foreground distance from the narrow H I absorption to the VLBI continuum source is not well constrained we suspect that it must be $>$ 100 pc given its narrow velocity width and the position stability of the its velocity centroid; if the gas was closer one would expect tidal forces to widen the velocity width and increase velocity centroid variations.

Physically the narrow H I observations could be related to a minor merging event, detected 400 pc South-West of the core (Canalizo et al., 2003). As a result of this interaction the narrow H I component could arise in a tidal tail of gas that is moving towards the nucleus. According to galaxy merger simulations (Bournaud et al., 2005) part of the progenitor's gas that gets expelled in tidal tails during a merging event will eventually fall back on the disk. The narrow component could also be connected to the giant infalling molecular cloud located 1.35 kpc to the North-West of the nucleus (Bellamy & Tadhunter, 2004). However, the projected distances from the core are rather different such that a direct connection is not obvious. Both of the above gas components are relatively large ($>$ 100 pc) and thus would be consistent with having fairly constant H I opacity over the whole VLBI structure.

Further progress with constraining the size and origin of the narrow H I absorption system might be made by making future sensitive (and high spectral resolution) e-MERLIN or EVLA observations to try to trace the narrow H I absorption further along the jet.

5. Summary

We have presented VLBA H I absorption data of the core region of Cygnus A. H I absorption is detected over a linear scale of 95 pc, but is seen mainly along the counter-jet and on the nucleus. The integrated spectrum can be well-fitted by two Gaussian profiles suggesting a broad (FWHM= 244 ± 22 km s^{-1}) and a narrow ($<$ 30 km s^{-1}) component. Modeling the data shows that the broad absorption occurs only against the counter-jet and not against the jet. Against the unresolved core the opacity is very low. The broad velocity component can be explained by a circumnuclear disk which has its highest opacity 45 mas away (in projection) from the black hole. The narrow velocity component can be explained as an infalling tidal tail, presumably left from a past minor merging event.

The radius at which H I absorption occurs can be constrained with the help of limits on the orientation of the disk. We find a relatively narrow range of possible parameters, resulting in an estimated radius of $\sim$ 80 pc for the peak opacity, a disk scale-height of about 20 pc and hence an opening angle of 14°. The offset between the centroid of the broad velocity component and the mean systemic velocity can be explained by a tilt of 19° of the disk axis compared to the jet axis.

Based on the derived geometry of the circumnuclear H I disk we derived physical properties of the H I: The minimum gas density is $n > 10^4$ cm^{-3} with a spin temperature $T_{\rm spin} < 740$ K. With the H I observations alone we cannot distinguish between models for the H I absorbing gas phase which are primarily atomic or molecular. However, we get a range for the total gas column density through the H I absorbing disk of 10^{23} cm^{-2} $< N <$ 10^{24} cm^{-2}. An upper limit on the gas mass within a radius of 80 pc is $M_{\rm gasdisk} = 10^8$ M$_\odot$, which is a factor 25 less than the black hole mass estimated by Tadhunter et al. (2003).

The circumnuclear torus in Cygnus A has an estimated fiducial radius $\sim$ 3 pc, which is a much smaller scale than our observed H I absorption. The estimated mass in the torus clouds ($6{\cdot}10^5$ M$_\odot$) is too low to power (alone) the source for 10^7–10^8 yr. In contrast the H I disk has enough mass to feed the AGN and replenish the torus clouds.

Higher sensitivity, broader band observations are needed to study the properties of the atomic circumnuclear disk in more detail, to search for a connection with the torus and to investigate whether the torus contains a (very broad, 2000 km s^{-1}wide velocity feature) H I absorption component. Higher spectral resolution e-MERLIN or EVLA observations of the narrow absorption component are needed to try to trace absorption further out along the jet to constrain its physical size.

Acknowledgements. This research was supported by the EU Framework 6 Marie Curie Early Stage Training programme under contract number MEST-CT-2005-19669 ESTRELA. JC acknowledges financial support from the Swedish Science Research Council. We wish to thank Joan Wrobel of NRAO for extensive help in setting up the phased VLA for VLBI observations at a nonstandard observing frequency.

References

Antonucci, R. 1993, ARA&A, 31, 473
Bahcall, J. N. & Ekers, R. D. 1969, ApJ, 157, 1055
Barvainis, R. & Antonucci, R. 1994, AJ, 107, 1291
Bellamy, M. J. & Tadhunter, C. N. 2004, MNRAS, 353, 105
Bournaud, F., Jog, C. J., & Combes, F. 2005, A&A, 437, 69
Canalizo, G., Max, C., Whysong, D., Antonucci, R., & Dahm, S. E. 2003, ApJ, 597, 823
Carilli, C. L., Perley, R. A., Dreher, J. W., & Leahy, J. P. 1991, ApJ, 383, 554
Conway, J. E. 1999, in Astronomical Society of the Pacific Conference Series, Vol. 156, Highly Redshifted Radio Lines, ed. C. L. Carilli, S. J. E. Radford, K. M. Menten, & G. I. Langston, 259–+
Conway, J. E. & Blanco, P. R. 1995, ApJ, 449, L131+
Elitzur, M. 2008, New Astronomy Review, 52, 274
Elitzur, M. & Shlosman, I. 2006, ApJ, 648, L101
Fanaroff, B. L. & Riley, J. M. 1974, MNRAS, 167, 31P
Fuente, A., Black, J. H., Martín-Pintado, J., et al. 2000, ApJ, 545, L113
Hardcastle, M. J., Evans, D. A., & Croston, J. H. 2009, MNRAS, 396, 1929
Hicks, E. K. S., Davies, R. I., Malkan, M. A., et al. 2009, ApJ, 696, 448
Impellizzeri, V., Roy, A. L., & Henkel, C. 2006, in Proceedings of the 8th European VLBI Network Symposium
Jackson, N., Tadhunter, C., & Sparks, W. B. 1998, MNRAS, 301, 131
Jaffe, W., Meisenheimer, K., Röttgering, H. J. A., et al. 2004, Nature, 429, 47
Jones, D. L., Tingay, S. J., Murphy, D. W., et al. 1996, ApJ, 466, L63+
Jones, D. L., Wehrle, A. E., Piner, B. G., & Meier, D. L. 2001, ApJ, 553, 968
Krichbaum, T. P., Alef, W., Witzel, A., et al. 1998, A&A, 329, 873
Krolik, J. H. & Lepp, S. 1989, ApJ, 347, 179
Lo, K. Y. 2005, ARA&A, 43, 625
Maloney, P. R., Hollenbach, D. J., & Tielens, A. G. G. M. 1996, ApJ, 466, 561
Morganti, R., Oosterloo, T., Struve, C., & Saripalli, L. 2008, A&A, 485, L5
Nenkova, M., Sirocky, M. M., Ivezić, Ž., & Elitzur, M. 2008a, ApJ, 685, 147
Nenkova, M., Sirocky, M. M., Nikutta, R., Ivezić, Ž., & Elitzur, M. 2008b, ApJ, 685, 160
Ogle, P. M., Cohen, M. H., Miller, J. S., et al. 1997, ApJ, 482, L37+
Padovani, P. & Urry, C. M. 1992, ApJ, 387, 449
Peck, A. B. & Taylor, G. B. 2001, ApJ, 554, L147
Privon, G. C. 2009, ArXiv e-prints
Salomé, P. & Combes, F. 2003, A&A, 412, 657
Schinnerer, E., Eckart, A., Tacconi, L. J., Genzel, R., & Downes, D. 2000, ApJ, 533, 850
Tadhunter, C. 2008, New Astronomy Review, 52, 227
Tadhunter, C., Marconi, A., Axon, D., et al. 2003, MNRAS, 342, 861
Tadhunter, C. N., Packham, C., Axon, D. J., et al. 1999, ApJ, 512, L91
Taylor, G. B. 1996, ApJ, 470, 394
Tristram, K. R. W., Raban, D., Meisenheimer, K., et al. 2009, A&A, 502, 67
van Langevelde, H. J., Pihlström, Y. M., Conway, J. E., Jaffe, W., & Schilizzi, R. T. 2000, A&A, 354, L45
Vermeulen, R. C., Readhead, A. C. S., & Backer, D. C. 1994, ApJ, 430, L41
Whysong, D. & Antonucci, R. 2004, ApJ, 602, 116
Young, A. J., Wilson, A. S., Terashima, Y., Arnaud, K. A., & Smith, D. A. 2002, ApJ, 564, 176